Biointerface Research in Applied Chemistry
Open-Access Journal (ISSN: 2069-5837)

Volume 16, Issue 3, 2026, 85
https://doi.org/10.33263/BRIAC163.085

Thermodynamic and Kinetic Studies of Fe^{3+} Sorption at the Biofunctional Interface of Glycine-Modified Silica Gel

Mohammed A. Al-Anber [1,*], Ahmed K. Hijazi [2], Idrees F. Al-Momani [3], Mo'tasem Al-Bayed [2], Aya Al-Matarneh [2], Malak AlJaafreh [4], Suresh Sagadevan [4], Zaid A. Al-Anber [5]

1 Department of Chemistry, Faculty of Sciences, Applied Science Private University, P.O. Box 166, Amman 11931, Jordan
2 Department of Chemical Sciences, Faculty of Arts and Science, Jordan University of Science and Technology, Irbid, Jordan
3 Department of Chemistry, Faculty of Sciences, Yarmouk University, Irbid, Jordan
4 Nanotechnology and Catalysis Research Center, University of Malaya, Kuala Lumpur 50603, Malaysia
5 Department of Chemical Engineering, Faculty of Engineering Technology, Al-Balqa Applied University, 11131 Amman, P.O. Box 15008, Jordan
* Correspondence: m_alanber@ASU.edu.jo;

Received: 3.01.2026; Accepted: 10.05.2026; Published: 15.06.2026

Abstract: Following the successful development of glycine-functionalized silica gel material (SG-Gly-Na^+) as an effective sorbent for Fe^{3+} ions, this study evaluates the sorption efficiency and mechanism under batch conditions. The material is systematically investigated with varying contact time, initial Fe^{3+} concentration (1 to 100 mg L^{-1}), pH (2 to 11), temperature (25 to 55°C), and adsorbent dosage (1–10 gL^{-1}), followed by kinetic and isotherm modeling. The sorption process is rapid, achieving equilibrium within 50 to 120 min and a maximum removal efficiency of ~ 99% at pH 7.0. Sorption kinetics followed the pseudo-second-order model ($R^2 \geq 0.99$), and the Arrhenius analysis yielded an activation energy of –43.43 kJ mol^{-1}, indicating that the rate constant decreases with increasing temperature, consistent with a diffusion-controlled process or a change in the rate-limiting step at higher temperatures. The sorption capacity (q_e) increased with temperature, reaching an experimental q_e = 24.95 mg g^{-1} at 45°C, confirming the endothermic nature of the process. Equilibrium data at 25°C were well described by the Langmuir isotherm ($R^2 \approx 0.998$), indicating monolayer adsorption on homogeneous sites. At higher temperatures (35–55°C), the Freundlich model became statistically applicable ($R^2 \geq 0.947$), reflecting a temperature-dependent shift in the sorption mechanism with contributions from heterogeneous surface interactions or multilayer adsorption. High removal efficiencies were achieved even at ambient temperature, highlighting the sorbent's energy efficiency. The SG-Gly-Na^+ material exhibits fast kinetics and favorable sorption capacity for Fe^{3+} ions under the studied conditions, supporting its further evaluation for potential water treatment applications.

Keywords: glycine-functionalized silica gel; Fe^{3+} sorption; kinetic modeling; pseudo-second-order; Langmuir isotherm; Freundlich isotherm; activation energy; water treatment.

1. Introduction

Heavy metal contamination in water poses serious risks to human health, particularly affecting the gastrointestinal tract and liver [1–5]. The presence of iron(III) ions exceeding 0.3 mg L^{-1} can impart a metallic taste and odor to water, and higher concentrations may pose health concerns [6]. According to the World Health Organization, while iron is not considered a primary health hazard, excessive intake can cause gastrointestinal distress [7, 8].

Among various physical-chemical treatment technologies [9-12], adsorption is particularly attractive due to its cost-effectiveness, efficiency, and simplicity [13]. Various functionalized materials have been explored, and silica gel (SG) stands out as a promising adsorbent owing to its high surface area and thermal stability. Modification of the SG surface with amino acids, such as glycine, introduces functional groups (amino and carboxyl) that can chelate metal ions, thereby enhancing sorption efficiency, capacity, and selectivity [14–15]. For instance, glycine--, diglycine--, and triglycine-functionalized silica gels have been used to prepare Cu-imprinted sorbents with high selectivity [16]. Al-Anber et al. studied the sorption and removal of aqueous Fe^{3+} and U(VI) ions using silica gel functionalized with tris(2-aminoethyl)amine (SG-TAEA-NH_2), achieving maximum removal yields of ca. 98% at low metal concentrations [17,18]. Similarly, amino-functionalized silica gel has been applied for Fe(II) removal [19]. Li and Liu modified silica gel with L-glutamic acid, which increased Zn^{2+} removal efficiency from 74% to 91% compared to unmodified silica [20]. Recently, mesoporous silica functionalized with glycine via a two-step synthesis showed high sorption capacities for Co(II) and Ni(II) [21].

Glycine was chosen as the functionalizing agent because it combines both an amino (–NH_2) and a carboxyl (–COO^-) group in a single small molecule, enabling cooperative chelation of Fe^{3+} ions through inner-sphere complexation. Compared to thiol- or simple amine-functionalized silicas, glycine provides additional oxygen donor atoms that are known to enhance the binding affinity for hard Lewis acids such as Fe^{3+} [14, 22, 23]. Moreover, the chemical stability of the amide linkage formed during immobilization ensures that the functional groups remain anchored under the aqueous conditions typical of wastewater treatment, while the hydrophilic nature of glycine promotes good dispersion of the sorbent. Unmodified silica gel, in contrast, lacks these specific binding sites and exhibits only weak, non-selective adsorption [22]. The combination of low cost, environmental friendliness, and strong metal-binding ability makes glycine-modified silica a promising alternative to conventional synthetic ion-exchange resins and other functionalized materials.

In our recent work [22], we reported the synthesis, characterization, and XAFS evidence for Fe^{3+} binding to glycine-functionalized silica gel (SG-Gly-Na^+). That study focused on structural elucidation and confirmed the formation of inner-sphere complexes. The present work extends that investigation by providing the first comprehensive kinetic, isotherm, and thermodynamic analysis of Fe^{3+} sorption onto SG-Gly-Na^+. It systematically evaluates the effects of pH, temperature, initial concentration, and sorbent dosage, and resolves earlier inconsistencies (e.g., the correct negative activation energy). Moreover, it reveals temperature-dependent shifts in isotherm behavior, highlighting the sorbent's multifunctional nature.

Building upon our recent report on the synthesis and characterization of glycine-functionalized silica gel (SG-Gly-Na^+) and the binding environment of Fe^{3+} within the matrix [22], the present work provides a detailed thermodynamic and kinetic analysis of Fe^{3+} sorption onto this material. Thermodynamic parameters are calculated to understand the spontaneity and nature of the process, while kinetic studies elucidate the sorption mechanism and rate-controlling steps. Both analyses are essential for designing and optimizing bio-functional sorbents for water treatment applications.

In this study, the sorption capacity and efficiency of SG-Gly-Na^+ toward Fe^{3+} ions are evaluated under varying pH, temperature, contact time, and initial concentration. Kinetic data are fitted to pseudo-first-order, pseudo-second-order, and intra-particle diffusion models. Equilibrium data are analyzed using the Langmuir and the Freundlich isotherms. The

adsorption performance of SG-Gly-Na^+ is compared with that of unmodified silica and other amino acid-functionalized silica materials reported in the literature. The results provide insight into the sorption mechanism, supporting the rational design of efficient biofunctional adsorbents for environmental applications.

2. Materials and Methods

2..1 Reagents.

All chemicals of Fe^{3+} ions source ($Fe(NO_3)_3$ $9H_2O$, Fluka Chemika, Germany), Sodium hydroxide (Sigma Aldrich, Germany) were of analytical reagent grade and used directly without further purification. A stock solution (1000 mg L^{-1}) of Fe^{3+} ion was prepared by dissolving a stoichiometric amount of $Fe(NO_3)_3.9H_2O$ in 1000 mL of ultrapure deionized water (18 Ωcm). The standard model solutions of 1-100 mg L^{-1} were prepared by appropriate dilution.

2.2. Instrumentation and analysis.

An Atomic Absorption Spectrophotometer (Varian Spectra AA 55, Perkin-Elmer, USA) was used to analyze the concentration of the Fe^{3+} ions in an aqueous solution. The pH of all solutions was recorded by a pH meter (Milwaukee Mi 150, Romania). The temperature was controlled using a temperature controller and an Isothermal shaker (Memmert, Germany). The analytical balance is used with ± 0.0001 mg (Sartorius, CP324-S/ management system certified according to ISO 9001).

2.3. Batch sorption process vs. variable parameters.

The sorption performance of SG-Gly$^-Na^+$ material toward the Fe^{3+} ion was tested by using a batch system at specific T = 25ºC (± 1ºC) with changing in C_i at 1, 5, 10, 25, and 50 mg L^{-1}; or at specific C_i at 50 mg L^{-1} with changing T at 25, 35, 45, and 55ºC. The closed sorption system containing 2 g L^{-1} SG-Gly$^-Na^+$ material was shaken vigorously (thermostatic mechanical shaker at 80 rpm) for up to 180 minutes. Afterward, the supernatant must be filtered through filter paper (Whatman No. 41). The filtrate can be analyzed. All experiments were performed in triplicate, and the results are reported as the mean value. The relative standard deviation (RSD) was ≤ 5% for all measurements, indicating good reproducibility.

The pH of the solution was adjusted using dilute solutions of 0.1 M HCl or 0.1 M NaOH, measured with a calibrated pH meter (Milwaukee Mi 150, Romania). No buffer was added to avoid any potential interference from complexing agents or competing cations. The pH was checked before the addition of the sorbent and, where necessary, readjusted to the target value (± 0.1 units) after the sorbent was introduced. For experiments investigating the effect of pH (Section 3.3), the pH was maintained at the desired value throughout the contact time by periodic monitoring and, if needed, minor adjustments with the same dilute acid or base solutions.

2.4. Equilibrium studies.

The amount of the adsorbed Fe^{3+} ion onto the SG-Gly$^-Na^+$ material at equilibrium and at a specific time *(t)* is q_e and q_t (mg g^{-1}); these are calculated by equations 1 and 2, respectively.

$$q_e = \frac{(C_i - C_e)}{S} \qquad (1)$$

$$q_t = \frac{(C_i - C_t)}{S} \qquad (2)$$

Where C_i, C_e, and C_t are the initial, equilibrium, and final concentrations of Fe^{3+} ions in the aqueous solution (mg L^{-1}), respectively. The dosage (S) of SG-$Gly^{-}Na^{+}$ material can be calculated by equation 3:

$$S = \frac{m}{v} \qquad (3)$$

Where v and m are the initial volume of Fe^{3+} ion solution and the mass of SG-$Gly^{-}Na^{+}$ material, respectively.

The percentage removal of Fe^{3+} ions can be calculated by equation 4:

$$\%\ Removal\ of\ Fe^{3+}\ \text{ion} = \frac{C_i - C_e}{C_i} \times 100\% \qquad (4)$$

3. Results and Discussion

3.1. Parametric investigation of Fe^{3+} ion sorption onto glycine-functionalized silica gel.

Recently, the binding environment of Fe^{3+} ions within the SG-$Gly^{-}Na^{+}$ matrix has been established [22]. Based on the reported structural and spectroscopic evidence, confirming strong inner-sphere coordination through carboxylate groups and Fe–O–Si linkages, the kinetic and sorption isotherms are evaluated. Thus, the sorption performance was evaluated under batch conditions at varying ion concentrations. Wherein, Fe^{3+} ions form an inner-sphere SG-$Gly^{-}Fe^{3+}$ complex through coordination with fabricated carboxylate and/or amine functional groups of glycine in the silica gel matrix. From another direction, ion exchanges between Fe^{3+} and Na^{+} ions take place.

The sorption efficiency of SG-Gly–Na^{+} towards Fe^{3+} ions is 70% (t = 90 minutes), compared to 10% unmodified SG-Cl material, as shown in Figure 1 [22]. This confirms that the SG-surface functionalization with glycine facilitates Fe^{3+} ion capturing. Wherein, the carboxylate (–COO^{-}) and secondary amine (–NH_2) functionalities are the main active sites for the sorption. It is reported that these functionalities can coordinate easily with Fe^{3+} ions through inner-sphere complexation with a surface-controlled chemisorption mechanism [23]. In comparison, the SG-Cl material has a poor performance due to the lack of these binding groups. Thus, it relies predominantly on weaker physisorption or non-specific interactions.

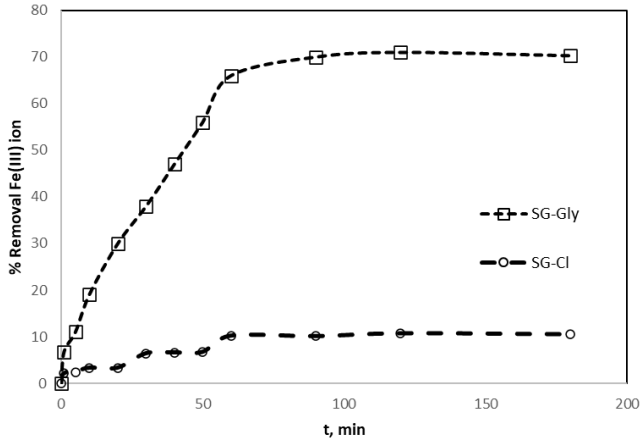

Figure 1. Time-dependent sorption of Fe^{3+} ions onto SG-Cl and SG-$Gly^{-}Na^{+}$ materials (C_i = 100 mg L^{-1}, T = 25°C, pH_i = 3, 80 rpm, 2 g L^{-1}, 100 – 250 µm) [22]. SG-Gly–Na^{+} exhibited significantly higher performance (≈70% removal at 90 min) compared to unmodified silica (~10%), confirming the role of carboxylate and amine groups in Fe(III) binding.

This behavior matches the reported findings of the high affinity and rapid reaction rates for heavy metal ions using amino acid-modified silica materials [24, 25]. It is noted that equilibrium was achieved within 90 minutes, indicating saturation of the sorbent's available binding sites. The analysis follows a pseudo-second-order kinetic model, implying a chemisorption-controlled process [26]. These studies demonstrate that introducing amino acid functionalities onto silica surfaces enhances sorption kinetics and binding strength. Both studies are consistent with the observed sorption performance of SG-Gly–Na^+ towards Fe^{3+} ions.

3.2. Influence of initial Fe^{3+} concentration on removal efficiency.

Figure 2 shows the effect of the initial concentration of Fe^{3+} ions on their sorption over SG-Gly$^-Na^+$ materials. In which initial concentrations range from 1 to 100 mg. L^{-1} is used at constant temperature (25 °C), unadjusted pH (pH_i = 3), and a shaking speed of 80 rpm. The observed results reveal that the percentage removal of Fe^{3+} ions decreases sharply with increasing initial concentration (C_i). The removal efficiency is 91% through using some diluted concentrations (1.00 mg L^{-1}). Wherein the active sites on the SG-Gly$^-Na^+$ surface are readily accessible, and there is less competition among ions. This allows for favorable and smooth diffusion of Fe^{3+} ions into the silica gel network. However, as concentrated solutions, a steep decline in removal efficiency is observed. For example, at 25 mg L^{-1}, the removal drops to about 10%, and this low efficiency remains relatively stable even at higher concentrations up to 100 mg L^{-1}. This decline can be attributed to the limited number of active sorption sites on the SG matrix and the increased competition among Fe^{3+} ions. At higher concentrations, the surface becomes saturated more quickly [27]. Also, general adsorption theory supports that when the number of adsorption sites is fixed, increasing the metal ion concentration leads to saturation and lower fractional uptake [28]. A more closely related system using chitosan functionalized with pyridine similarly demonstrated a plateau in Fe^{3+} uptake at high initial concentrations, consistent with site saturation [29].

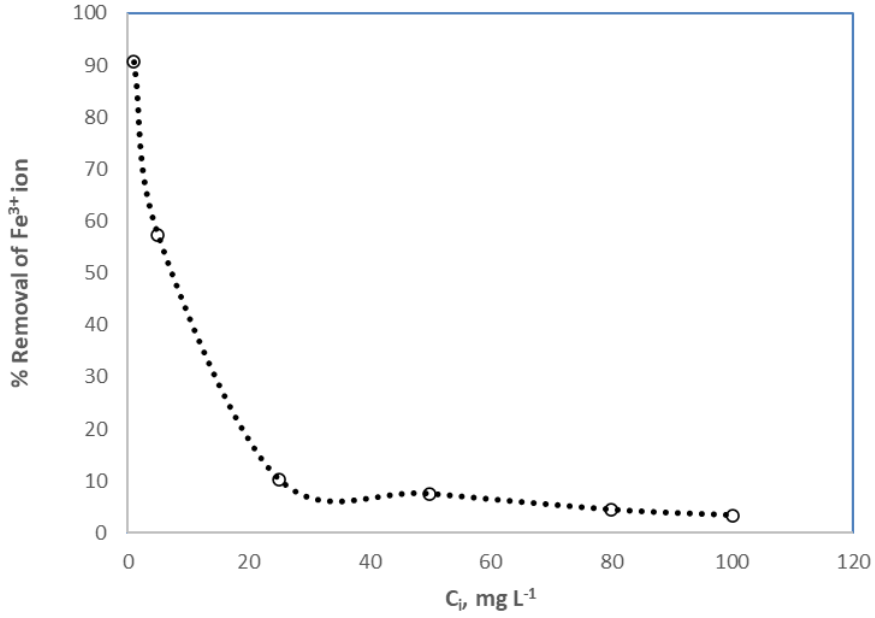

Figure 2. Influence of initial Fe^{3+} ion concentration on the percentage removal by SG-Gly$^-Na^+$. The removal efficiency decreases sharply with increasing initial concentration, indicating high sorption at low concentrations and reduced efficiency at higher concentrations (C_i = 1 - 100 mg L^{-1}, T = 25°C, pH_i = 3, 80 rpm, 2 g L^{-1}, t = 90 min., particle size =100 – 250 μm).

It should be noted that the data shown in Figure 2 were obtained under unadjusted, acidic conditions (pH ≈ 2.8), where proton competition severely limits Fe^{3+} binding. In contrast, the kinetic and isotherm experiments presented in Sections 3.6 – 3.8 were performed under optimized conditions (pH 5.0 – 7.0, longer contact times, and higher temperatures), where the material exhibits near-complete removal (≥ 99%) even at initial Fe^{3+} concentrations up to 50 mg L^{-1}. Thus, the concentration-dependent trend in Figure 2 reflects performance under non-optimal conditions and does not conflict with the high removal efficiencies observed under optimized conditions.

3.3. Influence of pH on Fe^{3+} removal efficiency.

The influence of solution pH on the sorption of Fe^{3+} ions onto SG-Gly^{-}Na^{+} was examined over a pH range of 2 to 11, with experimental conditions maintained at C_i = 100 mg L^{-1}, T = 25°C, 80 rpm, adsorbent dose of 2 g L^{-1}, particle size 100 – 250 µm, and a contact time of 90 minutes. The percentage removal of Fe^{3+} ions is highly dependent on pH, as shown in Figure 3. At low pH (pH = 2 – 4), the removal efficiency is significantly reduced, reaching 10 – 20 %. In this respect, protons (H^{+}) interfere with Fe^{3+} ion binding by occupying exchangeable Na^{+} sites on the SG-Gly-Na^{+} matrix. Thereby, H^{+} can suppress effective ion exchange or complexation. As the pH increases toward neutral (pH ~7), the removal efficiency rises sharply. This pH is considered an optimal condition for Fe^{3+} sorption, achieving a removal of 99 %. This can also be explained by the idea that proton interference is minimized. Wherein, the active sites of functional groups of glycine and modified silica gel are more available for binding with Fe^{3+} ions. From another direction, at pH > 7, a slight drop in removal efficiency is observed, stabilizing around 90%. This reduction is due to precipitation as $Fe(OH)_3$. Wherein, to distinguish between sorption and precipitation, control experiments without the sorbent were conducted under identical pH conditions. At pH values above 7, a slight decrease in Fe^{3+} concentration was observed in the blank solutions, which was attributed to the formation of $Fe(OH)_3$ precipitates. The sorption data reported in Figure 3 were corrected for this contribution, ensuring that the measured removal reflects true sorption onto SG-Gly-Na^{+} rather than hydrolysis products. This behavior matches that reported in similar studies using functionalized silica materials, such as tris(2-aminoethyl)amine- or glycine-modified silica gels [18, 22].

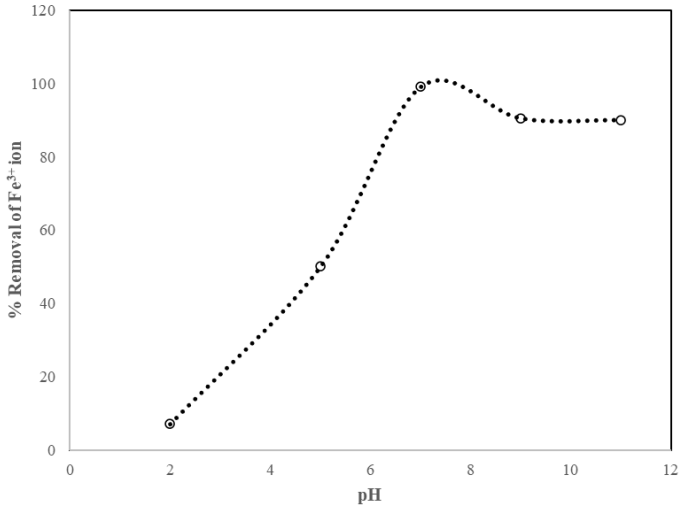

Figure 3. Effect of pH on the sorption of Fe^{3+} ions onto SG-Gly^{-}Na^{+} (C_i = 100 mg L^{-1}, T = 25°C, 80 rpm, adsorbent dose = 2 g L^{-1}, particle size = 100–250 µm, t = 90 min). Maximum removal of ~ 99% is observed at pH = 7, with lower efficiency at acidic pH.

3.4. Influence of temperature on Fe^{3+} removal efficiency.

In this target, the experiments are conducted at temperatures ranging from 25 to 55 °C. The other parameters are kept constant for pH = 6.0, 80 rpm, 2 g L^{-1} adsorbent dose, particle size 100–250 µm, and with two trials of constant initial Fe^{3+} concentrations of 1 mg L^{-1} or 50 mg L^{-1}. Figure 4 illustrates the results showing the percentage removal of Fe^{3+} ions that increases steadily with temperature, rising from 82% at 25 °C to 99% at 55 °C for the low initial concentration (1 mg L^{-1}). This means that higher temperatures can enhance the mobility and interaction of Fe^{3+} ions onto SG-Gly^{-}Na^{+} surface in diluted solution. wherein, it is known that higher thermal energy improves ion mobility/diffusion into active sites such as sorption of Fe^{3+}, Fe^{2+}, Ca^{2+}, and Zn^{2+} on manganese dioxide-modified green biochar [30]. In contrast, the removal efficiency remains consistently high ~100% across all temperatures at the higher initial concentration (50 mg L^{-1}). This indicates that no influence on the rising temperature. In this case, the sorption sites on the SG-Gly^{-}Na^{+} matrix are fully utilized, even at room temperature, when Fe^{3+} concentration is sufficiently high. The high efficiency of the SG-Gly^{-}Na^{+} and the energy-saving option (99 % at 25 °C) make it an effective material for catching iron ions, especially in large-scale applications where heating may not be feasible.

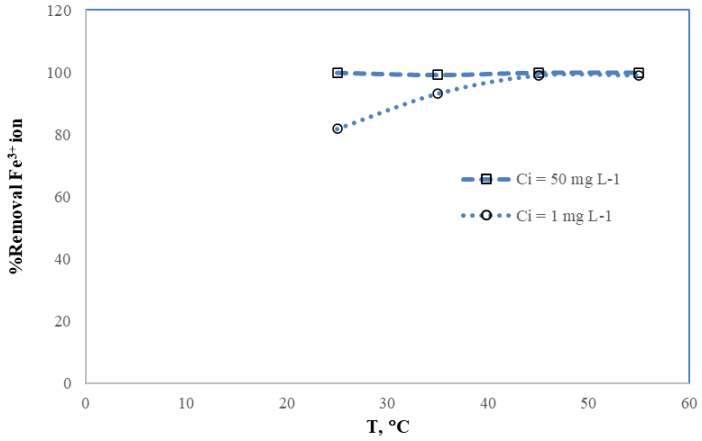

Figure 4. Effect of temperature on the sorption of Fe^{3+} ions onto SG-Gly^{-}Na^{+} at two initial concentrations (C_i = 1 and 50 mg L^{-1}), with T = 25–55 °C, 80 rpm, pH = 6, adsorbent dose = 2 g L^{-1}, t = 90 min, and particle size = 100–250 µm.

3.5. Influence of dosage on Fe^{3+} ion removal.

To investigate the influence of adsorbent dosage on the removal efficiency of SG-Gly^{-}Na^{+}, different dosages are used, ranging from 1 to 10 g L^{-1}, as shown in Figure 5. The obtained results reveal a significant increase in Fe^{3+} ion removal with increasing adsorbent dosage. It shows a steep increase in removal efficiency at lower dosages (1–5 g L^{-1}). This indicates that the SG-Gly^{-}Na^{+} material has a high sorption capacity and rapid uptake behavior. Wherein, as the dosage increases, more active sites become available for ion exchange and complexation with Fe^{3+} ions, leading to more efficient removal from the solution. The maximum removal efficiency (~ 100%) is achieved at a dosage of 10 g. L^{-1}, at which the matrix becomes fully loaded. The fast response to dosage changes suggests that SG-Gly^{-}Na^{+} possesses a strong affinity for Fe^{3+} ions, which is supported by the study of the removal of iron(III) ions using pyridine-modified chitosan [29, 31].

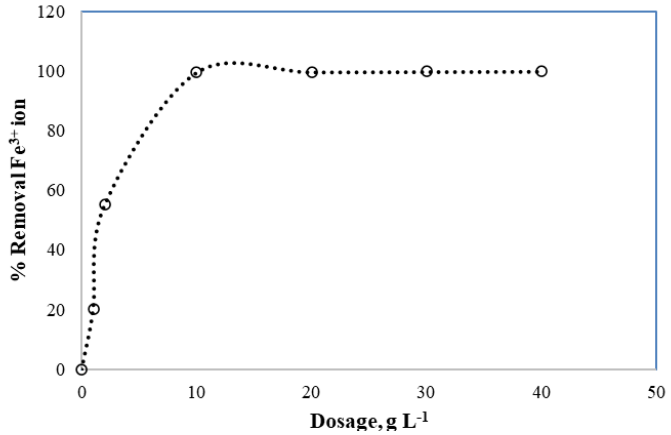

Figure 5. Effect of SG-Gly⁻Na⁺ dosage on the percentage removal of Fe^{3+} ions from aqueous solution (t = 90 min, T = 25 °C, pH = 5.0, 80 rpm, C_i = 100 mg L^{-1}).

3.6. Sorption kinetics of Fe^{3+} ions onto SG-Gly⁻Na⁺.

To investigate sorption kinetics, the effect of contact time was studied at different temperatures (25, 35, 45, and 55°C) with C_i = 50 mg L^{-1} and pH = 5.0, as shown in Figure 6. Across all temperatures, the removal rate of Fe^{3+} ions is initially rapid within the early stages of contact. This behavior is attributed to the availability of the primarily carboxylate and amine functional groups on the SG-Gly⁻Na⁺ surface, which facilitates strong coordination with Fe^{3+} ions. The equilibrium is reached after 90 minutes, with 90% removal, and maximum removal of ca. 99% within 120 minutes at 55°C. The improved sorption efficiency at elevated temperatures supports the suggestion that the sorption process is endothermic. This kinetic behavior is consistent with previous studies demonstrating rapid Fe^{3+} adsorption and equilibrium within 2 – 3 hours using modified silica gel materials [32], highlighting that the SG-Gly⁻Na⁺ material offers rapid and efficient Fe^{3+} removal, making it highly suitable for practical applications in water treatment where quick response and high performance are essential.

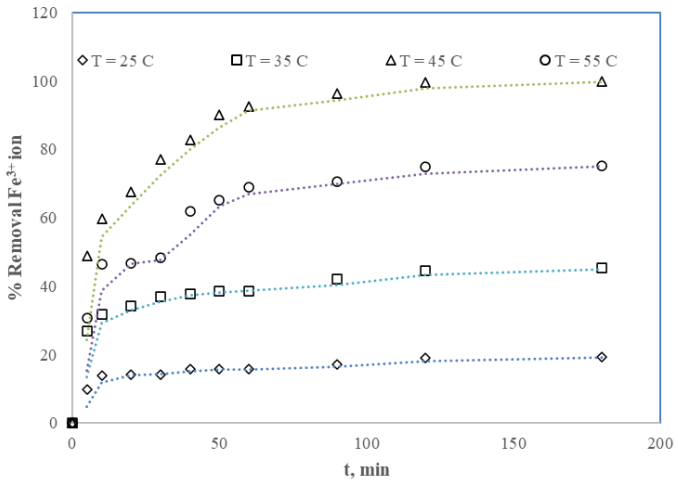

Figure 6. Effect of contact time and temperature on the sorption of Fe^{3+} ions onto SG-Gly⁻Na⁺ (C_i = 50 mg L^{-1}, T = 25–55 °C, pH = 5.0, 80 rpm, 2 g L^{-1} adsorbent dose, particle size = 100 – 250 µm). Rapid initial sorption occurs within 90 minutes, achieving up to 99% removal.

3.7. Kinetic modeling of Fe^{3+} sorption onto SG-Gly–Na⁺.

To understand the mechanism of Fe^{3+} sorption onto the SG-Gly⁻Na⁺ material and to analyze the sorption behavior, three widely accepted kinetic models were applied, such as the

Pseudo-first-order model (Lagergren), Pseudo-second-order model, and Elovich equation. These models were used in their linearized forms to determine the best fit to the experimental data. The best-fitting model can reveal the nature of the interaction between Fe^{3+} ions and the SG-$Gly^{-}Na^{+}$ adsorbent.

The pseudo-first-order model, originally proposed by Lagergren, assumes that the rate of occupancy of adsorption sites is proportional to the number of unoccupied sites. The model is expressed in differential and integrated forms as follows [33].

$$\frac{d_q}{d_t} = k_1(q_e - q_t) \quad (5)$$

$$\ln(q_e - q_t) = \ln q_e - k_1 t \quad (6)$$

Where, q_e and q_t (mg g^{-1}) are the amounts of sorbed Fe^{3+} ion at equilibrium and at any time (t), respectively, k_1 (min^{-1}) is the pseudo-first-order rate constant, and t (minutes) is the contact time.

The pseudo-second-order model assumes that the sorption process follows second-order chemisorption, involving valence forces through the sharing or exchange of electrons between the sorbent and the sorbate. It is more suitable for systems where chemisorption is the rate-limiting step. This model is expressed by equations 7 and 8 [34], which are considered for the sorption of metal ions into a solid matrix from the liquid solution:

$$\frac{d_q}{d_t} = k_2(q_e - q_t)^2 \quad (7)$$

$$\frac{t}{q_t} = \frac{1}{k_2 q_e^2} + \frac{t}{q_e} \quad (8)$$

Where: k_2 is the rate constant of the pseudo-second-order kinetic model (g mg^{-1} min^{-1}). The plot of t/q_t versus t gives a straight line with slope $1/q_e$ and an intercept of $1/(k_2 q_e^2)$. Figure 7 presents the pseudo-second-order kinetic model for the sorption of Fe^{3+} ions onto SG-$Gly^{-}Na^{+}$ at different temperatures ranging from 25°C to 55°C. The experimental conditions include Initial Fe^{3+} concentration (C_i) = 50 mg L^{-1}, pH = 5.0, Agitation speed = 80 rpm, dose = 2 g L^{-1}, Particle size = 100 – 250 µm. The plots of t/q_t *vs.* t show strong linearity at all temperatures, supporting the applicability of the pseudo-second-order kinetic model ($R^2 \geq 0.9916$).

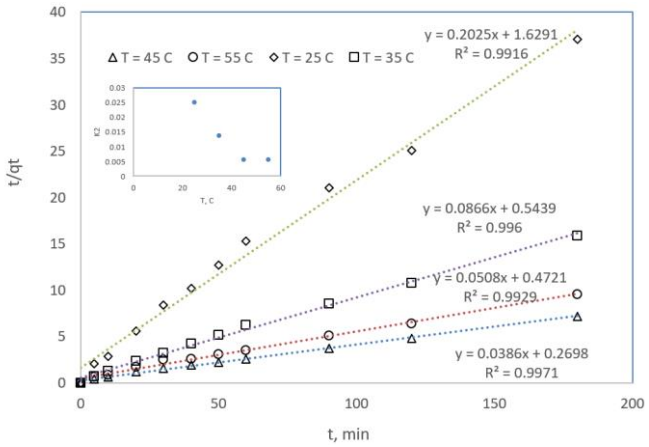

Figure 7. Kinetic plots of the pseudo-second-order model for the sorption of Fe^{3+} ions onto SG-$Gly^{-}Na^{+}$ at various temperatures (C_i = 50 mg L^{-1}, pH = 5.0, 80 rpm, T = 25 - 55 °C, adsorbent dose = 2 g L^{-1}, particle size = 100 – 250 µm). Data were fitted to a pseudo-second-order model to elucidate the mechanism of sorption.

The slopes of the lines decrease with rising temperature, reflecting an increase in the equilibrium capacity (q_e) at higher temperatures. The calculated rate constant k_2 decreases with temperature, as confirmed by the Arrhenius analysis (E_a = – 43.43 kJ mol^{-1}). This behavior is often associated with diffusion-controlled processes or a change in the rate-limiting step at elevated temperatures. Higher temperatures increase sorption capacity, indicating the endothermic nature of the sorption process. These observations are consistent with the pseudo-second-order model, which provides a good fit to the data. However, the negative activation energy suggests that a simple chemisorption mechanism does not govern the process under the conditions studied. These observations are consistent with previous studies reporting that the pseudo-second-order model accurately describes Fe^{3+} sorption kinetics and reflects chemisorption as the rate-controlling step [32, 34].

Table 1 provides a comprehensive summary of the pseudo-second-order kinetic parameters for the sorption of Fe^{3+} ions onto the SG-Gly^{-}Na^{+} adsorbent at varying temperatures (25–55°C). The parameters include: (i) Coefficient of determination (R^2), which measures how well the model fits the data, (ii) *Chi*-square error (χ^2), which indicates deviation between experimental and model-predicted values, (iii) Calculated and experimental sorption capacities ($q_{e,\,calc}$ and $q_{e,exp}$), and (iv) Pseudo-second-order rate constant (k_2). All R^2 values are very high (> 0.99), confirming that the pseudo-second-order model accurately fits the experimental kinetic data across all temperatures. The χ^2 values are low (0.016 – 0.045), supporting a good agreement between calculated and experimental q_e values. Similar findings have been reported in Fe^{3+} adsorption studies, where the pseudo-second-order model showed high correlation and strong agreement between $q_{e,\,\mathrm{calc}}$ and $q_{e,exp,}$ confirming chemisorption behavior driven by valence forces such as surface complexation or ion exchange [35]. The best model agreement (lowest χ^2: 0.0164) is observed at 35°C, suggesting this is the most favorable temperature in terms of both sorption efficiency and model predictability. The experimental sorption capacity $q_{e,\,exp}$ increases with temperature from 4.85 mg g^{-1} at 25°C to 24.95 mg g^{-1} at 45°C, indicating that the sorption is endothermic in nature. Comparable temperature-dependent increases in sorption capacity for Fe^{3+} have been reported in other adsorbent systems, where positive enthalpy changes ($\Delta H° > 0$) confirmed endothermic adsorption behavior [36]. A slight decrease in capacity (q_e) is observed at 55°C (18.81 mg.g^{-1}). This may be attributed to a partial weakening of the Fe^{3+}–ligand bonds at higher temperatures, leading to a marginally lower equilibrium loading, or to minor conformational changes in the glycine layer that reduce the number of accessible binding sites. To confirm the structural integrity of the sorbent, desorption experiments were performed at 55°C using 0.1 M HCl, which showed that > 95% of the sorbed Fe^{3+} could be recovered, indicating that the sorbent remains stable and the process is reversible. The reaction trend remains endothermic up to 45°C, while the slight decrease at 55°C suggests an optimal temperature range for practical application. The k_2 shows a decreasing trend with increasing temperature, from 0.0252 g·mg^{-1}·min^{-1} at 25°C to ~ 0.0055 g·mg^{-1}·min^{-1} at 55°C. This suggests that while sorption capacity increases with temperature, the sorption rate slows, likely because the system approaches equilibrium more gradually at higher temperatures.

The data imply that the sorption process is chemisorption, as expected for pseudo-second-order kinetics, involving valence forces (e.g., ion exchange or surface complexation). The optimal temperature ranges for Fe^{3+} removal appear to be between 35°C and 45°C, balancing high capacity and acceptable kinetics. The decreasing k_2 with increasing temperature suggests that sorption becomes more capacity-dominated rather than rate-limited at higher temperatures.

Table 1. Pseudo-second order parameters of sorption of Fe^{3+} ions into SG-Gly^{-}Na^{+} material using a temperature-controlled.

T (°C)	k_2 (g mg^{-1} min^{-1})	$q_{e,\,Exp}$ (mg g^{-1})	$q_{e,\,Calc}$ (mg g^{-1})	x^2	R^2
25	0.025171	4.8511	4.938272	0.017652	0.9916
35	0.013788	11.35743	11.54734	0.016447	0.9960
45	0.005522	24.95072	25.90674	0.036902	0.9971
55	0.005466	18.805	19.68504	0.044706	0.9929

$$x^2 = \frac{q_{cal} - q_{exp}}{q_{cal}}$$

Figure 8 is a linearized Arrhenius plot, which relates the pseudo-second-order rate constant (k_2) to temperature. It's used to estimate the activation energy (E_a) of the sorption process. The linear form of the Arrhenius equation is [37]:

$$\ln k_2 = -\frac{E_a}{R} . \left(\frac{1}{T}\right) + \ln A \qquad (9)$$

Where: k_2: pseudo-second-order rate constant (g mg^{-1} min^{-1}); T: temperature in Kelvin; R: universal gas constant (8.314 J mol^{-1} K^{-1}); E_a: activation energy (J mol^{-1}); ln A: intercept related to the frequency factor.

Figure 8 shows the Arrhenius model, with a strong correlation (R2 = 0.9643). Wherein the model fits the data well and indicates that temperature strongly influences the sorption rate. The calculated Activation Energy (E_a) is – 43.43 kJ/mol. The negative activation energy indicates that the rate constant k_2 decreases with increasing temperature, consistent with the kinetic data in Fig. 7. Such behavior is often associated with diffusion-controlled processes or a change in the rate-limiting step at higher temperatures. These findings suggest that Fe^{3+} sorption onto SG-Gly-Na^{+} is not governed by a simple chemisorption mechanism under the studied conditions, and that mass transport phenomena likely play a significant role.

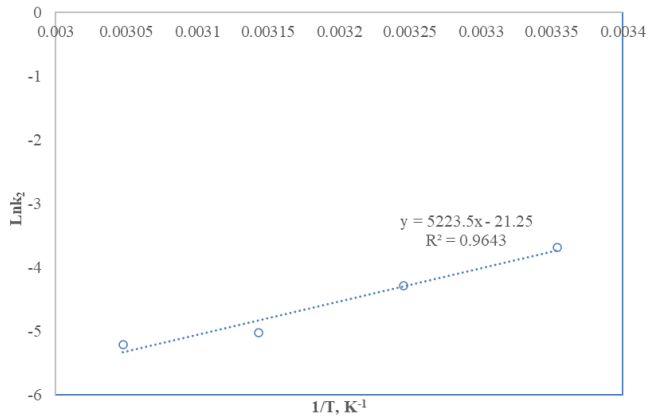

Figure 8. Arrhenius plot for the pseudo-second-order rate constant (k_2) of Fe^{3+} sorption onto SG-Gly^{-}Na^{+} at different temperatures. The linear relationship between lnk_2 and 1/T indicates temperature-dependent sorption kinetics. The calculated activation energy (E_a) is – 43.43 kJ mol^{-1}, indicating that k_2 decreases with increasing temperature, which is consistent with a diffusion-controlled process or a change in the rate-limiting step at higher temperatures rather than a simple chemisorption mechanism.

Figure 9 shows the kinetic plots of the pseudo-second-order model for the sorption of Fe^{3+} ions onto SG-Gly^{-}Na^{+} for various initial concentrations (C_i) ranging from 1 to 50 mg L^{-1}. At all concentrations, the initial stage of sorption (0 – 20 minutes) shows a steep increase in removal efficiency, especially for lower concentrations (1–20 mg L^{-1}). This rapid uptake is attributed to a high concentration gradient between Fe^{3+} ions and available carboxylate and amine functional groups on SG-Gly^{-}Na^{+}. Furthermore, the strong interactions and

complexation between Fe^{3+} and functional groups in the SG-$Gly^{-}Na^{+}$ matrix. Wherein, the sorption of Fe^{3+} onto SG-Gly-Na^{+} was rapid during the initial stages, with equilibrium attained within 20 min for all initial concentrations studied (1–50 mg L^{-1}). Therefore, a contact time of 20 min was selected for isotherm experiments to ensure equilibrium conditions. At low C_i (1–20 mg L^{-1}), near-complete removal, ca. 100 %, is achieved rapidly, within 30–50 minutes. This is due to an excess of active binding sites relative to available Fe^{3+} ions. At high C_i (50 mg L^{-1}), the removal efficiency increases more slowly, reaching ~ 90% at 50 minutes, and approaching ~ 99% after 120 minutes. This delay is due to increased competition for binding sites and possible saturation effects at higher ion concentrations. The equilibrium is generally reached after ~50 minutes for low concentrations and ~120 minutes for higher concentrations. The plateau phase beyond this point indicates saturation of adsorption sites and equilibrium sorption. Combined with the earlier pseudo-second-order kinetic modeling (Figures 10 and Table 3), this data strongly supports Pseudo-second-order kinetics, as indicated by higher R^2 values than for the pseudo-first-order model. This model assumes that chemisorption is the rate-limiting step, consistent with the observed behavior, suggesting electron sharing or exchange between Fe^{3+} and functional groups on SG-$Gly^{-}Na^{+}$. The observed trends are consistent with previously reported studies [27, 38], where Fe^{3+} sorption followed pseudo-second-order kinetics and showed strong dependence on C_i, with chemisorption being the dominant mechanism.

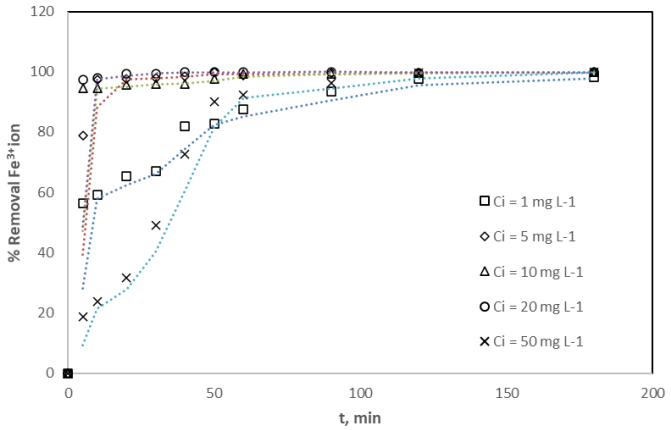

Figure 9. Effect of initial Fe^{3+} ion concentration (C_i = 1–50 mg L^{-1}) on the percent removal over time by SG-$Gly^{-}Na^{+}$. Experimental conditions: T = 25 °C, pH = 5.0, adsorbent dose = 2 g L^{-1}, particle size = 100–250 µm, 80 rpm. Faster removal is observed at lower concentrations (≥99%), with equilibrium achieved within 90 minutes.

Combined with the findings from earlier pseudo-second-order kinetic modeling (Figures 10 and Table 2), this data strongly supports Pseudo-second-order kinetics, as indicated by higher R^2 values ($R^2 \geq 0.9273$) compared to the pseudo-first-order model. Most R^2 values are ≥ 0.99, further supporting a chemisorption-based mechanism. This behavior is consistent with previous studies: for example, adsorption of Fe^{3+} onto a thiourea-crosslinked chitosan template followed pseudo-second-order kinetics, with a better fit than pseudo-first-order kinetics, and reached equilibrium within approximately 60 min [39].

As C_i increases, the slope of the line decreases. At 1 mg L^{-1}, steep slope, high t/q_t → low sorption capacity. While at 50 mg L^{-1}, Shallow slope, low t/q_t → high sorption capacity. This reflects that at higher initial concentrations, more Fe^{3+} is available to occupy the sorption sites, increasing the equilibrium capacity q_e. We observe that q_e increases with C_i, confirming that SG-$Gly^{-}Na^{+}$ has sufficient capacity to handle higher Fe^{3+} loads. k_2 tends to decrease with

increasing C_i, likely due to greater competition among Fe^{3+} ions for available active sites, slowing down individual adsorption events. The strong fit to the pseudo-second-order model and the concentration dependence of q_e are indicative of a chemisorption mechanism, involving electron sharing or exchange between Fe^{3+} ions and the amine/carboxylate functional groups in SG-Gly^{-}Na^{+}. This supports the hypothesis that the process is chemical rather than purely physical adsorption.

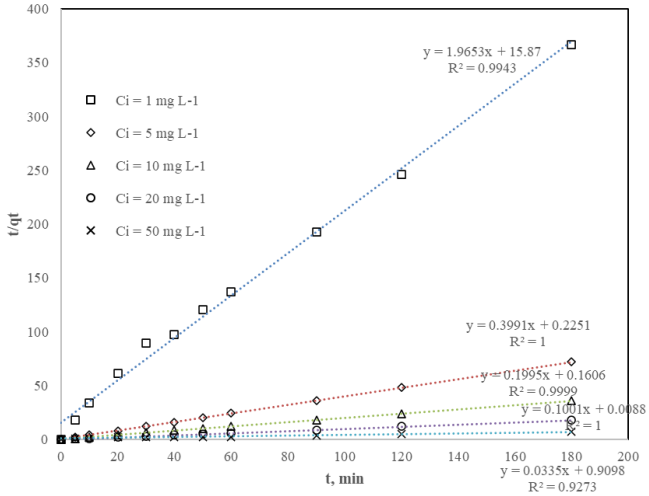

Figure 10. Pseudo-second-order kinetic plots (t/q_t vs. t) for the sorption of Fe^{3+} ions onto SG-Gly^{-}Na^{+} at varying initial concentrations (C_i = 1 – 50 mg L^{-1}). Experimental conditions: T = 25°C, pH = 5.0, adsorbent dose = 2 g L^{-1}, particle size = 100–250 µm, agitation speed = 80 rpm.

3.8. Sorption isotherm of Fe^{3+} on SG-Gly^{-}Na^{+}.

The equilibrium sorption data at 45 °C were analyzed using the Langmuir [40] and the Freundlich [41] isotherm models. All data points were obtained from initial Fe^{3+} concentrations of 1–50 mg L^{-1} under the following conditions: pH = 5.0, contact time = 90 min, adsorbent dose = 2 g L^{-1}, agitation speed = 80 rpm, and particle size = 100–250 µm.

The Langmuir model assumes monolayer coverage of Fe^{3+} ions on homogeneous sites of SG-Gly-Na^{+} at 45°C, combining all initial concentrations (1 – 50 mg L^{-1}), using the equation:

$$\frac{C_e}{q_e} = \frac{1}{q_{max}b} + \frac{1}{q_{max}} C_e \qquad (10)$$

Where q_{max} is the maximum capturing of Fe^{3+} ions per unit dosage of SG-Gly-Na^{+} composite (mg g^{-1}), and b is the Langmuir constant (L g^{-1}), which is exponentially related to the heat of adsorption and the affinity of binding sites. A plot of C_e/q_e vs. C_e (Figure 11) gives a poor linear fit (R^2 = 0.356), indicating that the sorption at 45°C does not follow ideal monolayer behavior. The calculated Langmuir parameters from the regression are q_{max} = 61.35 mg g^{-1} and b = 0.014 L mg^{-1}, but the low R^2 value makes these parameters unreliable.

The equilibrium sorption data at 25, 35, 45, and 55°C were analyzed using the Freundlich isotherm model; representative results at 45°C are shown in Figure 12, using the equation:

$$\ln q_e = \ln K_F + \left(\frac{1}{n}\right) \ln C_e \qquad (11)$$

where K_F (mg g^{-1} (L mg^{-1})$^{1/n}$) is the Freundlich constant related to sorption capacity, and n is an empirical constant related to sorption intensity (favorability). The linearized plot of

lnq_e vs. lnC_e (Figure 12) exhibits excellent linearity (R^2 = 0.9935) with the regression equation lnq_e = 0.8264lnC_e + 5.8695. The n = 1.21 > 1 indicates favorable adsorption, and the intercept gives K_F = 354 mg g^{-1} (L mg^{-1})$^{1/n}$. The high R^2 value confirms that the Freundlich model accurately describes the equilibrium at 45°C, suggesting that the sorption involves multilayer interactions on a heterogeneous surface. These results are consistent with the sorption of metal ions into amine-functionalized silica [18], amino-functionalized cross-linked chitosan [42], amino-functionalized mesoporous silica [43], and tris(2-aminoethyl)amine moiety functionalized silica gel [17]. Wherein, higher temperatures enhance diffusion and promote multilayer interactions on heterogeneous surfaces [44].

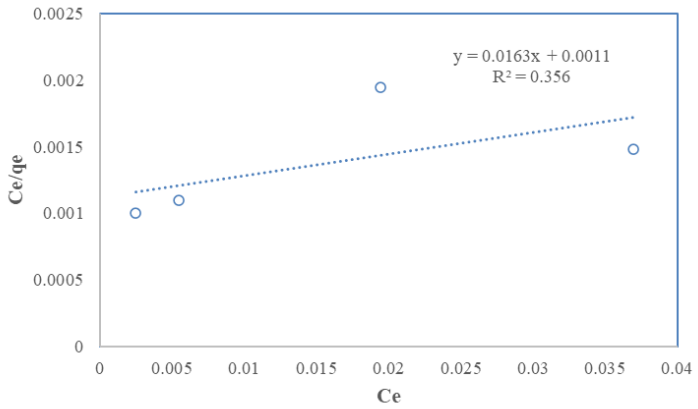

Figure 11. Linearized Langmuir isotherm plot (C_e/q_e vs. C_e) for the sorption of Fe^{3+} onto SG-Gly-Na^+ at 45°C. Data points were obtained from experiments with initial Fe^{3+} concentrations ranging from 1 to 50 mg L^{-1}. Experimental conditions: pH = 5.0, contact time = 90 min, adsorbent dose = 2 g L^{-1}, agitation speed = 80 rpm, particle size = 100–250 µm.

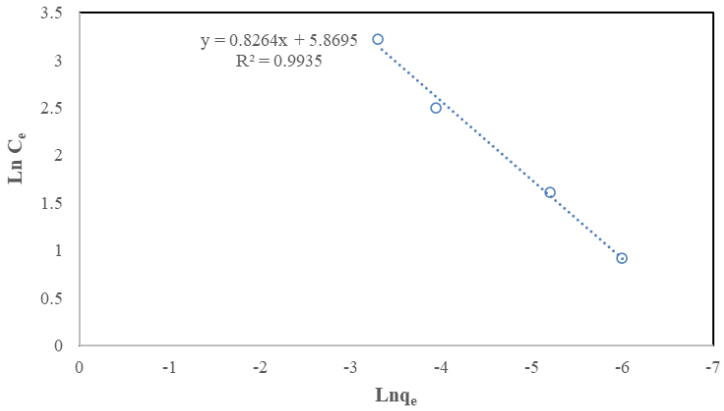

Figure 12. Linearized Freundlich isotherm plot (Ln q_e *vs.* Ln C_e) for the sorption of Fe^{3+} onto SG-Gly-Na^+ at 45°C. Data points were obtained from experiments with initial Fe^{3+} concentrations ranging from 1 to 50 mg L^{-1}. Experimental conditions: pH = 5.0, contact time = 90 min, adsorbent dose = 2 g L^{-1}, agitation speed = 80 rpm, particle size = 100–250 µm.

4. Conclusion

Glycine-functionalized silica gel (SG-Gly-Na^+) demonstrates high efficiency and strong affinity for Fe^{3+} ions under the studied conditions. Sorption behavior depends on initial concentration, sorbent dosage, pH, and temperature. Maximum removal efficiency (ca. 99%) is achieved near neutral pH ≈ 7, where proton competition is minimized; lower efficiencies at acidic pH and slight declines at alkaline pH are attributed to proton interference and $Fe(OH)_3$ precipitation, respectively. Sorption kinetics follow the pseudo-second-order model (R^2 ≥

0.99), which is often associated with chemisorption. However, the negative activation energy (E_a = −43.43 kJ mol^{-1}) indicates that the rate constant decreases with increasing temperature, pointing to a diffusion-influenced process or a change in the rate-limiting step at elevated temperatures. Equilibrium data at 25°C fit the Langmuir isotherm well ($R^2 \approx 0.998$), suggesting monolayer adsorption on homogeneous binding sites. At higher temperatures (35–55°C), the Freundlich model becomes statistically acceptable ($R^2 \geq 0.947$), indicating that additional contributions from heterogeneous surface interactions or multilayer adsorption become detectable. Our finding, SG-Gly^-Na^+ exhibits rapid kinetics, favorable equilibrium behavior, and good sorption capacity for Fe^{3+} removal under optimized conditions. These findings support its further development as a functional sorbent for aqueous iron remediation. However, additional studies involving competitive ions and real-water matrices would be necessary to assess its practical applicability.

Author Contributions

Conceptualization, M.A.A.; methodology, M.A.A. and A.K.H.; investigation, M.B.M. and A.A.M.; formal analysis, I.F.A.; validation, M.A.A., A.K.H. and I.F.A.; data curation, M.B.M. and A.A.M.; writing—original draft preparation, M.A.A.-A.; writing—review and editing, M.A.J. and I.F.A.; visualization, M.A.A.; supervision, M.A.A. and A.K.H.; project administration, M.A.A.; resources, A.K.H. and S.S.; funding acquisition, M.A.A. and A.K.H. All authors have read and agreed to the published version of the manuscript.

Institutional Review Board Statement

Not applicable.

Informed Consent Statement

Not applicable.

Data Availability Statement

All data generated or analyzed during this study are included in this published article.

Funding

This research received no external funding.

Acknowledgments

The authors, AKH and MAA, would like to thank the Deanship of Scientific Research for financial support through Jordan University of Science and Technology (Research grant # 20190401) and Applied Science Private University (research grant # DRGS/2025/5).

Conflicts of Interest

The authors declare that they have no competing interests.

References

1. Liu, P.; Borrell, P.F.; Božič, M.; Kokol, V.; Oksman, K.; Mathew, A.P. Nanocelluloses and their phosphorylated derivatives for selective adsorption of Ag^{+}, Cu^{2+} and Fe^{3+} from industrial effluents. *J. Hazard. Mater.* **2015**, *294*, 177-185, https://doi.org/10.1016/j.jhazmat.2015.04.001.
2. Sarin, P.; Snoeyink, V.; Bebee, J.; Jim, K.; Beckett, M.; Kriven, W.; Clement, J. Iron release from corroded Iron pipes in drinking water distribution systems: effect of dissolved oxygen. *Water Res.* **2004**, *38*, 1259–1269, https://doi.org/10.1016/j.watres.2003.11.022.
3. Das, B.; Hazarika, P.; Saikia, G.; Kalita, H.; Goswami, D.; Das, H.; Dube, S.; Dutta, R. Removal of Iron from groundwater by ash: A systematic study of a traditional method. *J. Hazard. Mater.* **2007**, *141*, 834–841, http://dx.doi.org/10.1016/j.jhazmat.2006.07.052.
4. Viessman Jr., W.; Hammer, M.J.; Perez, E.M.; Chadik, P.A. Water Supply and Pollution Control, 8th Edition; Pearson Education Limited: Essex, **2008**.
5. Kontoghiorghes, G.J.; Weinberg, E.D. Iron: Mammalian defense systems, mechanisms of disease, and chelation therapy approaches. *Blood Rev.* **1995**, *9*, 33-45, https://doi.org/10.1016/0268-960x(95)90038-1.
6. Who. Guidelines for drinking-water quality, volume 2: Health criteria and other supporting information: WHO, Geneva, 1985, ix + 333 pp. Price: Sw. fr. 35.00. *Sci. Total Environ.* **1987**, *61*, 274, https://doi.org/10.1016/0048-9697(87)90388-3.
7. World Health, O. Guidelines for drinking water quality 4th edition incorporating the first addendum. *Acceptability Aspects: Taste, Odour And Appearance, Geneva* **2017**, 224-226.
8. Zamzow, M.J.; Murphy, J.E. Removal of Metal Cations from Water Using Zeolites. *Sep. Sci. Technol.* **1992**, *27*, 1969-1984, https://doi.org/10.1080/01496399208019459.
9. Lee, M.S.; Nicol, M.J. Removal of iron from cobalt sulfate solutions by ion exchange with Diphonix resin and enhancement of iron elution with titanium(III). *Hydrometallurgy* **2007**, *86*, 6-12, https://doi.org/10.1016/j.hydromet.2006.10.002.
10. Andersen, W.C.; Bruno, T.J. Application of a gas–liquid entraining rotor to supercritical fluid extraction: Removal of iron(III) from water. *Anal. Chim. Acta* **2003**, *485*, 1-8, https://doi.org/10.1016/S0003-2670(03)00400-8.
11. Sivakami, G.; Priyadarshini, R.; Baby, V.; Rajakumar, S.; Ayyasamy, P.M. Bioremediation of Ferric Iron in Synthetic Metal Oxide Using *Bacillus* Sp. (SO-10). *J. Curr. Perspect. Appl. Microbiol.* **2012**, *1*, 34–41.
12. Alıcılar, A.; Meriç, G.; Akkurt, F.; Şendil, O. Air Oxidation of Ferrous Iron in Water. *J. Int. Environ. Appl. Sci.* **2008**, *3*, 409–414.
13. Al-Anber, M.; Al-Anber, Z. Utilization of natural zeolite as ion-exchange and sorbent material in the removal of Iron. Desalination 2008, 225, 70–81, https://doi.org/10.1016/j.desal.2007.07.006.
14. Majewski, P.; Albrecht, T.; Weber, S. COOH-functionalisation of silica particles. Appl. Surf. Sci. 2011, 257, 9282–9286, https://doi.org/10.1016/j.apsusc.2011.04.145.
15. Yantasee, W.; Rutledge, R.D.; Chouyyok, W.; Sukwarotwat, V.; Orr, G.; Warner, C.L.; Warner, M.G.; Fryxell, G.E.; Wiacek, R.J.; Timchalk, C.; Addleman, R.S. Functionalized Nanoporous Silica for the Removal of Heavy Metals from Biological Systems: Adsorption and Application. *ACS Appl. Mater. Interfaces* **2010**, *2*, 2749-2758, https://doi.org/10.1021/am100616b.
16. Bi, X.; Lau, R.J.; Yang, K.-L. Preparation of Ion-Imprinted Silica Gels Functionalized with Glycine, Diglycine, and Triglycine and Their Adsorption Properties for Copper Ions. *Langmuir* **2007**, *23*, 8079-8086, https://doi.org/10.1021/la7008072.
17. Zaitoun, M.A.; Al-Anber, M.A.; Al Momani, I.F. Sorption and removal aqueous iron(III) ion by tris(2-aminoethyl)amine moiety functionalized silica gel. *Int. J. Environ. Anal. Chem.* **2020**, *100*, 1446-1467, https://doi.org/10.1080/03067319.2019.1654466.
18. Al-Anber, M.A.; Al-Momani, I.F.; Zaitoun, M.A.; Al-Qaisi, W. Inorganic silica gel functionalized tris(2-aminoethyl)amine moiety for capturing aqueous uranium (VI) ion. *J. Radioanal. Nucl. Chem.* **2020**, *325*, 605-623, https://doi.org/10.1007/s10967-020-07270-x.
19. Nuengmatcha, P.; Saengsane, N.; Teppaya, N.; Rattanakomon, N.; Nuengmatcha, P. Iron removal from synthetic aqueous solution using amino functionalized commercial silica gel as adsorbent. *J. Appl. Sci. Emerg. Technol.* **2017**, *16*, 1-7, https://doi.org/10.14416/j.appsci.2017.10.S01.
20. Li, Y.; Liu, S. Synthesis of l-glutamic acid containing silica gel for the adsorption and immobilization of Zn2+ in water. Monatsh. Chem. 2019, 150, 1349–1354, https://doi.org/10.1007/s00706-019-02393-8.

21. Piątek, J.; de Bruin-Dickason, C.N.; Jaworski, A.; Chen, J.; Budnyak, T.; Slabon, A. Glycine-functionalized silica as sorbent for cobalt(II) and nickel(II) recovery. *Appl. Surf. Sci.* **2020**, *530*, 147299, https://doi.org/10.1016/j.apsusc.2020.147299.
22. Al-Anber, M.A.; Harfouche, M.; Hijazi, A.K.; Sobola, D.; Al-Bayed, M.t.; Al-Adaileh, N.; Sagadevan, S. Development and Analysis of Glycine-Modified Silica Gel for Efficient Fe^{3+} Ion Capture: Exploring Synchrotron XAFS Insights. *Biointerface Res. Appl. Chem.* **2025**, *15*, 61, https://doi.org/10.33263/BRIAC155.061.
23. Biyun, S.; Yifan, H.; Li, W.; Xiaoteng, L.; Dandan, P.; Tingyu, Y.; Ao, Z.; Faida, P.; Liqing, D. The Syntheses, Characterization and Crystal Structures of a Series of Heterocyclic β-Diketones and Their Isoxazole Compounds. *Curr. Org. Synth.* **2019**, *16*, 1174-1184, https://doi.org/10.2174/1570179416666191022113022.
24. Saleem, M.U.; Hussain, H.; Shukrullah, S.; Yasin Naz, M.; Irfan, M.; Rahman, S.; Ghanim, A.A.J. Study of Kinetics and the Working Mechanism of Silica-Coated Amino-Functionalized $CoFe_2O_4$ Ferrite Nanoparticles to Treat Wastewater for Heavy Metals. *ACS Omega* **2024**, *9*, 3507-3524, https://doi.org/10.1021/acsomega.3c07200.
25. Irfan, M.; Zaheer, F.; Hussain, H.; Naz, M.Y.; Shukrullah, S.; Legutko, S.; Mahnashi, M.H.; Alsaiari, M.A.; Ghanim, A.A.; Rahman, S.; Alshorman, O.; Alkahtani, F.S.; Khan, M.K.A.; Kruszelnicka, I.; Ginter-Kramarczyk, D. Kinetics and Adsorption Isotherms of Amine-Functionalized Magnesium Ferrite Produced Using Sol-Gel Method for Treatment of Heavy Metals in Wastewater. *Materials* **2022**, *15*, 4009, https://doi.org/10.3390/ma15114009.
26. Abbou, B.; Lebkiri, I.; Ouaddari, H.; Kadiri, L.; Ouass, A.; Habssaoui, A.; Lebkiri, A.; Rifi, E.H. Removal of Cd (II), Cu (II), and Pb (II) by adsorption onto natural clay: a kinetic andthermodynamic study. *Turk. J. Chem.* **2021**, *45*, 362-376, https://doi.org/10.3906/kim-2004-82.
27. Satchawan, S.; Phuengphai, P.; Ratanamanee, A.; Meethong, N. Kinetic and Equilibrium Studies of Fe(III) Sorption from an Aqueous Solution Using Palmyra Palm Fruit Fibres as a Biosorbent. *Appl. Sci.* **2022**, *12*, 10540, https://doi.org/10.3390/app122010540.
28. Li, J.; Dong, X.; Liu, X.; Xu, X.; Duan, W.; Park, J.; Gao, L.; Lu, Y. Comparative Study on the Adsorption Characteristics of Heavy Metal Ions by Activated Carbon and Selected Natural Adsorbents. *Sustainability* **2022**, *14*, 15579, https://doi.org/10.3390/su142315579.
29. Zhang, L.; Liu, H.; Zhu, J.; Liu, X.; Li, L.; Huang, Y.; Fu, B.; Fan, G.; Wang, Y. Effective Removal of Fe (III) from Strongly Acidic Wastewater by Pyridine-Modified Chitosan: Synthesis, Efficiency, and Mechanism. *Molecules* **2023**, *28*, 3445, https://doi.org/10.3390/molecules28083445.
30. Maneechakr, P.; Karnjanakom, S. Environmental surface chemistries and adsorption behaviors of metal cations (Fe^{3+}, Fe^{2+}, Ca^{2+} and Zn^{2+}) on manganese dioxide-modified green biochar. *RSC Adv.* **2019**, *9*, 24074–24086, https://doi.org/10.1039/C9RA03112J.
31. Igberase, E.; Mkhize, I.G. Pyridine-modified chitosan for removal of Fe(III) ions: kinetics, equilibrium, and thermodynamics. Polymers 2023, 15, 1699, https://doi.org/10.3390/molecules28083445.
32. Zhang, S.; Niu, Y.; Chen, Z.; Chen, H.; Yang, Z.; Bai, L.; Yuan, B. Removal of Fe(III) from ethanol by silica-gel supported ester-terminated PAMAM dendrimers: experimental and DFT calculation. *Desalin. Water Treat.* **2019**, *164*, 310-318, https://doi.org/10.5004/dwt.2019.24455.
33. Lagergren, S. Zur Theorie der sogenannten Adsorption gelöster Stoffe. *Z. Chem. Ind. Kolloide* **1907**, *2*, 15-15, https://doi.org/10.1007/BF01501332.
34. Ho, Y.S.; McKay, G. Pseudo-second order model for sorption processes. *Process Biochem.* **1999**, *34*, 451-465, https://doi.org/10.1016/S0032-9592(98)00112-5.
35. Fatima, N.; Zhang, Q.; Chen, R.; Yan, D.; Zhou, Q.; Lu, X.; Xin, J. Adsorption Thermodynamics and Kinetics of Resin for Metal Impurities in Bis(2-hydroxyethyl) Terephthalate. *Polymers* **2020**, *12*, 2866, https://doi.org/10.3390/polym12122866.
36. Gunorubon, A.J.; Chukwunonso, N. Kinetics, Equilibrium and Thermodynamics Studies of Fe^{3+} Ion Removal from Aqueous Solutions Using Periwinkle Shell Activated Carbon. *Adv. Chem. Eng. Sci.* **2018**, *8*, 49–66, https://doi.org/10.4236/aces.2018.82004.
37. Atkins, P.; de Paula, J. Atkins' Physical Chemistry, 10^{th} Edition; Oxford University Press: Oxford, **2014**.
38. Baltakys, K.; Zadaviciute, S.; Eisinas, A. Adsorption kinetic parameters of Fe^{3+} and Ni^{2+} ions by gyrolite. *Mater. Sci.* **2015**, *21*, 117-122, https://doi.org/10.5755/j01.ms.21.1.5735.
39. Dai, J.; Ren, F.; Tao, C. Adsorption Behavior of Fe(II) and Fe(III) Ions on Thiourea Cross-Linked Chitosan with Fe(III) as Template. *Molecules* **2012**, *17*, 4388-4399, https://doi.org/10.3390/molecules17044388.

40. Langmuir, I. The adsorption of gases on plane surfaces of glass, mica and platinum. *J. Am. Chem. Soc.* **1918**, *40*, 1361–1403, https://doi.org/10.1021/ja02242a004.
41. Freundlich, H.M.F. Over the Adsorption in Solution. *Z. Phys. Chem.* **1906**, *57*, 385–471.
42. Igberase, E.; Mkhize, I.G. Amino-functionalized grafted cross-linked chitosan beads for the efficient adsorption of Pb^{2+} and Cu^{2+} ions in a synthetic media: equilibrium, kinetic, thermodynamic, and desorption study. *J. Iran. Chem. Soc.* **2025**, *22*, 1849-1862, https://doi.org/10.1007/s13738-025-03262-4.
43. Aguado, J.; Arsuaga, J.M.; Arencibia, A.; Lindo, M.; Gascón, V. Aqueous heavy metals removal by adsorption on amine-functionalized mesoporous silica. *J. Hazard. Mater.* **2009**, *163*, 213-221, https://doi.org/10.1016/j.jhazmat.2008.06.080.
44. El-Rayyes, A.; Arogundade, I.; Ofudje, E.A.; Refat, M.S.; Alsuhaibani, A.M.; Akande, J.A.; Sodiya, E.F. Thermodynamic, isotherm and kinetic studies lead ions adsorption onto *Manihot esculenta* chaff surface. *Sci. Rep.* **2025**, *15*, 27672, https://doi.org/10.1038/s41598-025-09307-1.

Publisher's Note & Disclaimer